Photoionization and heating of a supernova-driven turbulent interstellar medium

J. E. Barnes,[1][*] Kenneth Wood,[1] Alex S. Hill[2] and L. M. Haffner[3,4]

[1]*School of Physics & Astronomy, University of St Andrews, North Haugh, St Andrews, Fife KY16 9SS, Scotland*

[2]*CSIRO Astronomy & Space Science, Marsfield, NSW 1710, Australia*

[3]*Department of Astronomy, University of Wisconsin Madison, 475 North Charter Street, Madison, WI 53706, USA*

[4]*Space Science Institute, 4750 Walnut Street, Suite 205, Boulder, CO 80301, USA*

ABSTRACT

The diffuse ionized gas (DIG) in galaxies traces photoionization feedback from massive stars. Through three-dimensional photoionization simulations, we study the propagation of ionizing photons, photoionization heating and the resulting distribution of ionized and neutral gas within snapshots of magnetohydrodynamic simulations of a supernova-driven turbulent interstellar medium. We also investigate the impact of non-photoionization heating on observed optical emission line ratios. Inclusion of a heating term which scales less steeply with electron density than photoionization is required to produce diagnostic emission line ratios similar to those observed with the Wisconsin Hα Mapper. Once such heating terms have been included, we are also able to produce temperatures similar to those inferred from observations of the DIG, with temperatures increasing to above 15 000 K at heights $|z| \gtrsim 1$ kpc. We find that ionizing photons travel through low-density regions close to the mid-plane of the simulations, while travelling through diffuse low-density regions at large heights. The majority of photons travel small distances ($\lesssim 100$ pc); however some travel kiloparsecs and ionize the DIG.

Key words: ISM: General – galaxies: ISM.

1 INTRODUCTION

The interstellar medium (ISM) is a vital component of the cycle of star formation and the evolution of galaxies. The composition and dynamics of the ISM determine the formation of new stars in the Galaxy, while stars provide feedback through ionization, outflows and supernovae (Mac Low & Klessen 2004). In this paper, we study the formation of widespread ionized gas as observed primarily through Hα in the Milky Way and other galaxies. This gas (reviewed by Haffner et al. 2009), commonly referred to as the diffuse ionized gas (DIG) or warm ionized medium, is low density ($\lesssim 0.1$ cm^{-3}), warm ($\sim$8000 K), consists of regions of nearly fully ionized hydrogen (Hausen et al. 2002) and has a scaleheight of 1–1.5 kpc near the Sun (Haffner, Reynolds & Tufte 1999; Gaensler et al. 2008; Savage & Wakker 2009).

The most likely sources of the ionization of the DIG in the Galaxy are O stars (Reynolds 1990). Photoionization simulations of a smooth ISM are able to reproduce some of the observed properties of the DIG (e.g. Wood & Mathis 2004; Miller & Cox 1993). However, to allow ionizing photons from mid-plane OB stars to propagate to large distances, these models require the vertical column density of hydrogen to be lower than that inferred from HI 21 cm observations of the Galaxy. Photoionization simulations of a clumpy or fractal density structure show that the introduction of lower density paths in a three-dimensional (3D) ISM allows photons to travel to large heights above the mid-plane (see for example fig. 16 of Haffner et al. 2009). The most likely source of such clumping is turbulence (e.g. Armstrong, Rickett & Spangler 1995; Hill et al. 2008; Chepurnov & Lazarian 2010; Burkhart, Lazarian & Gaensler 2012) which could be driven by supernovae (e.g. Armstrong et al. 1995; de Avillez 2000; Mac Low & Klessen 2004). Wood et al. (2010) demonstrated that in a 3D supernova-driven turbulent medium, ionizing photons are indeed able to propagate to large distances and produce the DIG. However, the width of the distribution of emission measure in these simulations is wider than observed in the Galaxy. The discrepancy appears to be due to too wide a variation of density with height, requiring a mechanism to smooth out the density variations in the dynamical simulations. One possible smoothing mechanism is pressure from magnetic fields. In this paper, we extend the work of Wood et al. (2010) to study photoionization of a supernova-driven turbulent magnetized ISM, using the 3D density structures from the magnetohydrodynamic (MHD) simulations of Hill et al. (2012a).

Our simulations naturally produce a vertically extended ionized component and a compact neutral layer of gas, in qualitative

[*] E-mail: jb652@st-andrews.ac.uk

agreement with observations. However, the Hα intensity from the ionized layer has a smaller scaleheight than observed in the Galaxy. To better reproduce Hα observations in the Galaxy, we have created models of a 3D fractal ISM which provide estimates for the density structure and column densities for future MHD simulations. We also investigate the distance travelled by ionizing photons in the ISM and find that the majority of photons travel only short distances and only a small fraction need to travel kiloparsec distances to ionize the DIG.

The outline of the paper is as follows: a description of observations of the DIG is given in Section 2. The MHD and Monte Carlo photoionization codes are briefly described in Section 3, the results of our simulations are presented in Section 4 and are compared with observations of the DIG in the Galaxy. In Section 5, we describe the results of photoionization models of a 3D fractal ISM. In Section 6, we investigate how far photons are able to travel through the ISM to create the DIG. Finally, our conclusions are presented in Section 7.

2 WISCONSIN Hα MAPPER

Although the DIG was first detected at radio frequencies (Hoyle & Ellis 1963), much of our knowledge of its properties come from observations of optical emission lines (see review by Haffner et al. 2009). In our present study, we utilize data from the Wisconsin Hα Mapper (WHAM) survey which has mapped the entire northern sky in Hα (Haffner et al. 2003) and large sections in other optical emission lines including Hβ, [N II] λ6584 Å and [S II] λ6716 Å (Haffner et al. 1999; Madsen & Reynolds 2005; Madsen, Reynolds & Haffner 2006), and targeted observations of [O I] λ6300 Å (Reynolds et al. 1998; Hausen et al. 2002) and [O III] λ5007 Å (Madsen & Reynolds 2005). These observations provide information on the distribution, kinematics, and physical conditions in the DIG (Haffner et al. 1999; Haffner et al. 2003). Some of the main results from WHAM are that the temperature of the gas appears to increase with height from the mid-plane, inferred from the increase of [N II]/Hα and [S II]/Hα with height. Similar trends in line ratio and temperature have also been observed in other galaxies (e.g. Rand 1998; Otte, Gallagher & Reynolds 2002).

We take advantage of the kinematic information provided by WHAM to compare our photoionization simulations with observations of regions of the Galaxy with different star formation rates, namely gas associated with the Perseus Arm and an interarm region. The gas associated with the Perseus Arm is taken to be in the velocity range -75 km s^{-1} < V_{lsr} < -45 km s^{-1} and Galactic coordinate range $l = 125°$ to $156°$ and $b = -6°$ to $-35°$. There is some uncertainty as to the velocity of Hα associated with the Perseus Arm with other authors taking the arm to be in the range -50 km s^{-1} < V_{lsr} < -30 km s^{-1} (Haffner et al. 1999). We use an interarm region in the solar neighbourhood which lies in the velocity range -15 km s^{-1} < V_{lsr} < 15 km s^{-1} and Galactic coordinate range $l = 120°$ to $160°$ and $b = -30°$ to $30°$ (Madsen et al. 2006). These regions were observed as part of the WHAM Northern Sky Survey and are seen clearly in Hα emission (Madsen et al. 2006). In addition to Hα, maps of these regions in the [N II] λ6584 Å and [S II] λ6716 Å lines provide information on the temperature and ionization state of the gas up to 2 kpc above the mid-plane of the Galaxy (Haffner et al. 1999; Madsen et al. 2006; Madsen & Reynolds 2005).

3 MODELS

In this section, we briefly describe the MHD and Monte Carlo photoionization codes used in our theoretical study of diffuse ionized gas in the Galaxy.

3.1 Magnetohydrodynamic simulations

We investigate the structure of DIG photoionized by OB stars using a 3D density structure from supernova-driven MHD simulations of the ISM (Hill et al. 2012b). These simulations use FLASH v2.5 (Fryxell et al. 2000) and are based on those of Joung & Mac Low (2006) and Joung, Mac Low & Bryan (2009). A brief description of the simulations follows.

The density grid we use is from the magnetized 'bx50hr' simulation described by Hill et al. (2012a) which employs an adaptive mesh grid with maximum resolution of 2 pc near the mid-plane and lower resolution at $|z| \gtrsim$ 50–300 pc. The 'bx50hr' model has an initial uniform horizontal magnetic field of 6.5 µG in the mid-plane which approaches an rms value of 5–6 µG (see review by Kulsrud & Zweibel 2008). The full simulation grid is $1 \times 1 \times 40$ kpc, with the mid-plane situated at the centre of the box.

The MHD simulations use a modified version of the Kuijken & Gilmore (1989) gravitational potential which includes a stellar disc, spherical dark matter halo, and a Navarro, Frenk & White (1996) profile above $|z| = 8$ kpc. Supernova explosions drive turbulence and structure the ISM, while heating and cooling establish a multiphase, vertically stratified ISM. The supernovae are set off at approximately the Galactic supernova rate used by Joung et al. (2009): Type Ia = 6.58 Myr^{-1} kpc^{-2}, core collapse = 27.4 Myr^{-1} kpc^{-2}. Three fifths of the core-collapse supernovae are clustered spatially and temporally to simulate super bubbles, though supernova positions and times are determined without knowledge of the gas distribution. For our photoionization simulation, we consider a snapshot at $t = 316$ Myr.

These simulations include a diffuse heating term representing photoelectric heating by dust grains (Wolfire et al. 1995). They also contain heating terms from supernova explosions and stellar winds. photoionization is not considered and therefore heating by this mechanism is not included. Radiative cooling is incorporated as appropriate for an optically thin, solar metallicity plasma in collisional ionization equilibrium.

Since these simulations do not include photoionization, they are unable to distinguish between the warm ionized and neutral medium. The thermal pressure for a given density and temperature in the DIG is $\approx$2 times that in the warm neutral medium due to the extra electron associated with each H atom. However, the impact of this on the dynamics should be small because in 10^4 K gas the thermal pressure is significantly smaller than the turbulent pressure. Additionally, simulations of high-mass stars have shown that ionizing radiation is able to produce molecular outflows. However, the properties of the outflows suggest that ionizing radiation is not the main driver (Peters et al. 2012).

Fig. 1 shows horizontally averaged density from the MHD simulation as a function of height (z). We also show a Dickey–Lockman distribution for neutral hydrogen in the Galaxy (Dickey & Lockman 1990) and a Dickey–Lockman plus vertically extended component, as required to match the observed Hα in the Galaxy (Reynolds, Haffner & Tufte 1999). Although the average vertical column density for the MHD models (3.1×10^{20} cm^{-2}) is similar to that of the Dickey–Lockman distribution (2.9×10^{20} cm^{-2}), the MHD density
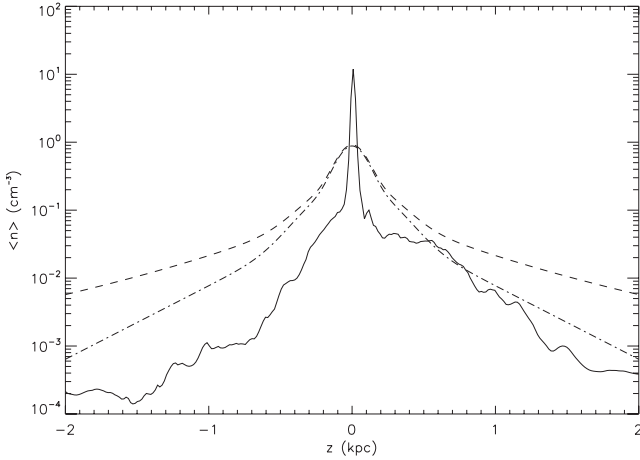
Figure 1. Mean density (solid line) from MHD simulations, Dickey–Lockman density (dot–dashed line) and Dickey–Lockman plus vertically extended gas component (dashed line). The MHD simulation has densities ≈ 100 times lower at $|z| = 2$ kpc and is much more sharply peaked than the average density structure required to produce the observed scaleheight of Hα in the Galaxy.

is more centrally peaked and is considerably lower at large $|z|$. As we will discuss in Section 4, the MHD density structure affects the scaleheight of Hα emission, temperature, and the line ratios [N II]/Hα and [S II]/Hα from the photoionization models.

3.2 Photoionization models

In order to determine how ionizing photons propagate and ionize the DIG, we use the 3D Monte Carlo photoionization code of Wood, Mathis & Ercolano (2004). This model follows ionizing photons through a 3D Cartesian grid and computes the temperature and ionization state of H, He, C, S, N, O, and Ne in each cell. Ionization from both direct stellar and diffuse photons from recombinations of H$^+$ and He$^+$ are included. Previous studies (e.g. Wood et al. 2010) indicate that the impact of dust on photoionization in the low-density DIG is minimal and has therefore been neglected. We adopt the following abundances appropriate for the diffuse ISM: He/H = 0.1, C/H = 1.4×10^{-4}, N/H = 6.5×10^{-5}, O/H = 4.3×10^{-4}, Ne/H = 1.17×10^{-4}, and S/H = 1.4×10^{-5}. The O/H and N/H abundances are averages from Jenkins (2009) and Simpson et al. (2004), S/H is taken from Daflon et al. (2009), He/H and Ne/H are from Mathis (2000).

For the photoionization simulations, we use a section of the MHD grid that extends ±2 kpc from the mid-plane. Memory restrictions of our photoionization code on a desktop computer require us to rebin the density grid and reduce the resolution to 15.6 pc per grid cell. We have explored higher spatial resolution ionization simulations for small sections of the grid as well as binning according to density-squared (because of the recombination rate dependence). The resulting local ionization and temperature structures are unchanged at the 5 per cent level compared to the lower resolution runs. This resolution does not allow us to study the small scale ionization of individual H II regions within the larger ISM grid. Therefore, the sources of ionizing radiation in our simulation represent radiation escaping from H II regions into the large-scale ISM and can be thought of as 'leaky H II regions' (e.g. Zurita, Rozas & Beckman 2000; Zurita et al. 2002). The sources are randomly

distributed in the *xy* plane, and their *z* location is randomly sampled from a Gaussian distribution with a scaleheight of 63 pc, the observed scaleheight of O stars in the Galaxy (Maíz-Apellániz 2001). Heating is from photoionization of the gas while cooling comes from recombination, free–free radiation, and collisionally excited line radiation from C, N, O, Ne, and S. We ignore the temperature structure from the MHD simulations, taking the density grid and calculating the temperature of the gas based only on heating by photoionization plus an additional heating term (as required to explain emission line ratios in the gas).

We randomly place 24 sources in our simulations, following the study by Garmany, Conti & Chiosi (1982) who estimated the surface density of O stars in the solar neighbourhood to be 24 stars kpc^{-2}. The sources are distributed uniformly in *x* and *y*, with *z* chosen to reproduce the scaleheight of O stars in the Galaxy (Maíz-Apellániz 2001). The stars within 2.5 kpc of the Sun have a total estimated Lyman continuum luminosity $Q = 7 \times 10^{51}$ s^{-1} (Garmany et al. 1982), while the total ionizing luminosity of the stars in the Galaxy is estimated to be 2.6×10^{53} s^{-1} (Williams & McKee 1997). Some ionizing photons will produce the DIG, some will escape the Galaxy altogether, and the remainder will be trapped and produce local H II regions around each source. As mentioned earlier, the small-scale H II regions are not studied in this paper. We equally distribute the ionizing luminosity among the 24 sources and investigate total luminosities escaping from H II regions $0.5 < Q_{49} < 10$, where $Q_{49} \equiv Q/(10^{49} \text{s}^{-1})$. As expected, the ionizing luminosity required to produce the DIG in our simulations is smaller than the total budget estimated by Vacca, Garmany & Shull (1996) of $Q_{49} \approx 35$ for all stars in 1 kpc^2 of the disc. Like the dynamical simulations which produce the density grid, the radiation transfer simulation has repeating boundary conditions where photons that leave the simulation box from the *x* or *y* faces re-enter the box on the opposite side. The ionizing spectrum is taken from the library of radiation-driven wind atmosphere models for hot stars computed by Pauldrach, Hoffmann & Lennon (2001) and Sternberg, Hoffmann & Pauldrach (2003). The spectrum used for these simulations is from a model atmosphere with solar abundance, $\log g = 3.4$ and $T = 35\,000$ K.

For an input density structure from the MHD simulations, we calculate the ionization and temperature structure arising from pure photoionization. We do not include photoelectric heating or shock heating, the two heating effects included in the MHD simulations. Therefore, the very high temperatures ($\sim 10^6$ K) in some regions of the MHD simulations are not accounted for in the photoionization models. Such regions represent the hot ionized medium component of the ISM (McKee & Ostriker 1977; Cox 2005) and have a volume filling factor of around 60 per cent in the sub-grid from the MHD simulation (i.e. $|z| < 2$ kpc), in good agreement with other observational and theoretical studies of the ISM (e.g. McKee & Ostriker 1977; Harfst, Theis & Hensler 2006). Since Hα emissivity is proportional to $T^{-0.9}$ (Osterbrock & Ferland 2006) and the gas is at very low density, the very hot regions will produce very low Hα intensity and can be ignored when computing the total intensity maps from the photoionization models. We have produced Hα maps with and without emission from the hot cells from the MHD simulation; they are almost identical for the reasons we have outlined. However, the low Hα intensity and high temperature of these cells makes analysis of our results more difficult. Therefore, in the following analysis the intensity and line ratio maps from the photoionization models do not include emission from the regions in the MHD simulations that have $T > 30\,000$ K.
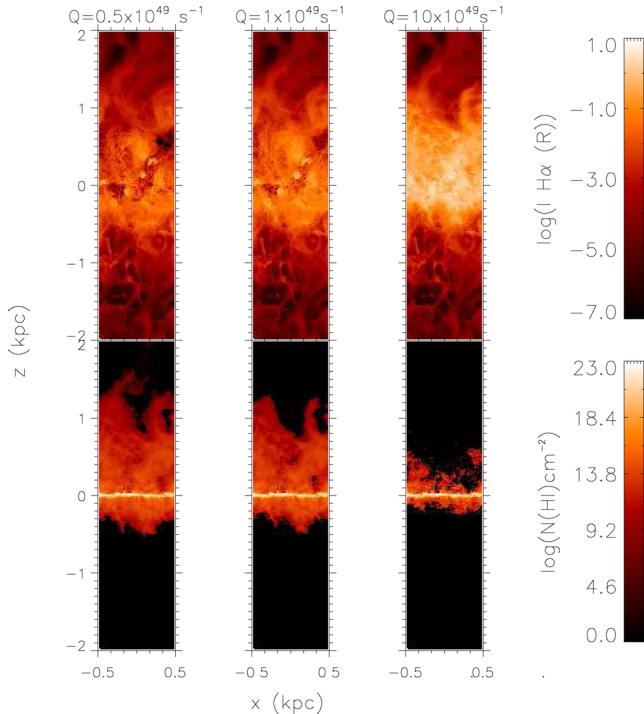
Figure 2. Edge on view of Hα intensity (top row) and column density of neutral hydrogen (bottom row) shown for increasing ionizing luminosity, $Q_{49} = 0.5$ (left), 1 (centre), 10 (right).

4 RESULTS

Fig. 2 shows maps of Hα intensity and column density of neutral hydrogen for different ionizing luminosities in our simulations. As in Wood et al. (2010), the photoionization simulations naturally produce ionized gas at all heights and a less vertically extended distribution of neutral hydrogen. As the ionizing luminosity is increased, the vertical extent of the neutral hydrogen decreases. These general properties are in qualitative agreement with observations in the Milky Way and many other galaxies.

Reynolds (1990) estimated that approximately 12 per cent of the ionizing photons from OB stars are required to support the ionization of the DIG. We find that a luminosity of $1 \lesssim Q \lesssim 10 \times 10^{49}$ s^{-1} is able to ionize hydrogen to heights of ±2 kpc and produce a compact distribution of neutral gas. This implies that for our simulations, around 3–28 per cent of the estimated Lyman continuum budget of $Q_{49} \approx 35$ for 1 kpc^2 (Vacca et al. 1996) is required to escape from H II regions to ionize the DIG. Similarly to Wood et al. (2010), we find that the most important parameter is the ionizing luminosity and that the position of the sources has little effect on ionization of the gas at large |z|. A fraction of the photons in our simulations, typically less than a few per cent, escape the simulation grid altogether (i.e. beyond $z = ±2$ kpc) and represent the escape fraction of ionizing photons into the intergalactic medium. Recent galaxy-wide simulations estimate the escape fraction of ionizing photons from dwarf galaxies into the IGM to be in the range 0.08 and 5.9 per cent (Kim et al. 2013), while Barger, Haffner & Bland-Hawthorn (2013) find that up to 4 per cent of ionizing photons escape from the SMC while up to 5.5 per cent escape from the LMC, encompassing the values from our study.

Fig. 3 shows that the scaleheight of Hα intensity from the MHD model is smaller than observed in the Milky Way. For simulations with $Q_{49} = 10$, the Hα scaleheight is 150 pc while for $Q_{49} = 1$

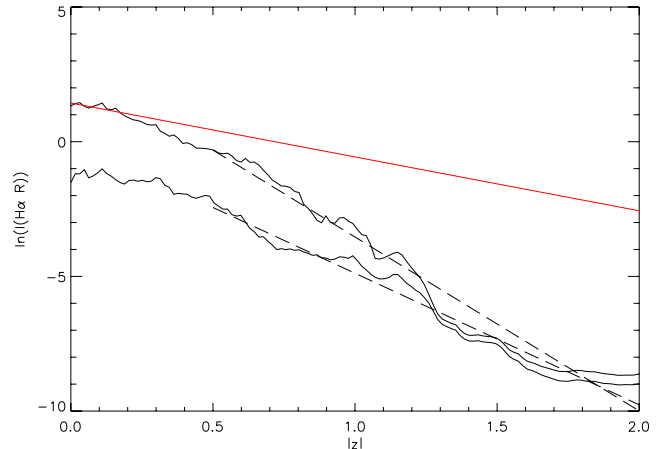**Figure 3.** Fit to the horizontally averaged Hα intensity versus height observed in the Perseus Arm (red), compared with photoionization models from Fig. 2. Top line: $Q_{49} = 10$ and a fit to the region of the model corresponding to observations of the Perseus Arm (dashed line); bottom line $Q_{49} = 1$ and fit (dashed line). The scaleheight of Hα intensity for the Perseus Arm is 500 pc. The simulations have scaleheights of 150 pc ($Q_{49} = 10$) and 250 pc ($Q_{49} = 1$). The Hα intensity close to the mid-plane is small for $Q_{49} = 1$ because this low ionizing luminosity produces a smaller fraction of ionized gas close to the dense mid-plane regions compared to models with higher ionizing luminosity.
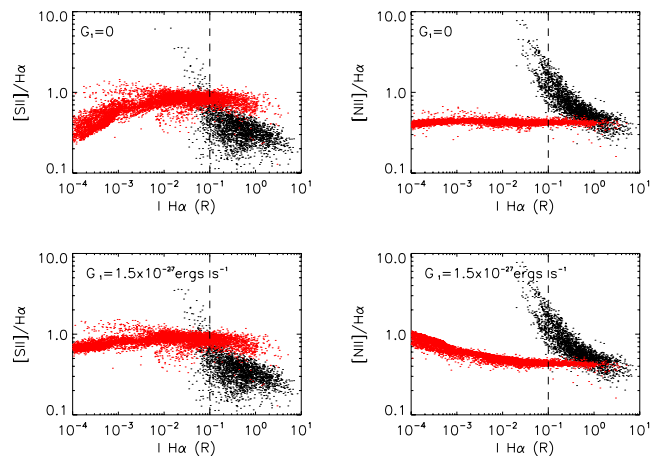

Figure 4. Emission line ratios showing [N II]/Hα versus Hα intensity for MHD simulations with $Q_{49} = 1$ (red points) compared with WHAM data from the Perseus Arm (black points). The vertical line represents the WHAM sensitivity limit. Upper and lower panels show simulations without and with additional heating, respectively.

it is 250 pc. These Hα scaleheights are smaller than the typical 500 pc observed in the Milky Way because of the lower scaleheight of the input density grid. Compared to low-Q models, in the high-Q models there is more ionized gas and hence a larger Hα intensity at small |z| and a smaller Hα scaleheight (see Figs 2 and 4).

4.1 Emission line ratios in the DIG

Observations of [S II]/Hα and [N II]/Hα in the DIG show that these line ratios increase with decreasing Hα intensity (Haffner et al. 1999) while [S II]/[N II] remains almost constant. It has been suggested that variations in temperature could explain the observed line ratios (e.g. Bland-Hawthorn, Freeman & Quinn 1997), with a higher temperature increasing [S II]/Hα and [N II]/Hα while keeping

[S II]/[N II] constant as result of the similar excitation potentials of S and N (Reynolds et al. 1999). The observed increase of [S II]/Hα and [N II]/Hα with altitude (Haffner et al. 2009) suggests a temperature in the DIG that increases with $|z|$ and requires additional physical processes that heat the gas in addition to photoionization. To provide additional heating in the low-density gas at high $|z|$, these sources of heating should have a shallower dependence on density than the n_e^2 dependence of photoionization heating. Possible mechanisms include heating from the dissipation of turbulence (proportional to n_e, Minter & Spangler 1997) and cosmic ray heating (proportional to $n_e^{-1/2}$; Wiener, Zweibel & Oh 2013).

Following the nomenclature in previous papers (Reynolds et al. 1999; Wood & Mathis 2004; Wiener et al. 2013), the heating/cooling equation can be written as

$$G_0 n_e^2 + G_1 n_e + G_3 n_e^{-1/2} = \Lambda n_e^2 , \qquad (1)$$

where the heating from photoionization (G_0) and the cooling function (Λ) are computed explicitly in our code. For these simulations, we introduce one additional heating term $G_1 n_e$ erg cm^{-3} s^{-1}, which will dominate over photoionization heating at low values of n_e. In the analytic fractal density structures considered in Section 5, we also consider additional heating from cosmic rays with the term $G_3 n_e^{-1/2}$ erg cm^{-3} s^{-1}.

Figs 4 and 5 show diagnostic line ratio plots of [S II]/Hα and [N II]/Hα versus Hα from our simulations without (top panels) and with (bottom panels) additional heating $G_1 n_e$. In Fig. 4, we compare the models to observations of the Perseus Arm, restricting the models to heights $|z| < 1.8$ kpc. Fig. 5 compares our models to observations of the lower star formation rate interarm region. Without additional heating, the [S II]/Hα and [N II]/Hα line ratios show little variation with Hα intensity and certainly no indication of the observed increase of the line ratios towards low Hα intensities. Including an additional heating term with $G_1 = 1.5 \times 10^{-27}$ erg s^{-1} does raise the [N II]/Hα, but only at extremely small Hα intensities.

It is important to note that the MHD simulations were performed for the average galactic supernova rate from Joung et al. (2009) with Type Ia and core collapse rates of 6.58 and 27.4 Myr^{-1} kpc^{-2}. The supernova rate is likely to be higher in the Perseus Arm where stars are forming. It is therefore appropriate to compare the simulated line ratios with an interarm region where the star formation and

supernova rate will be closer to the average rates for the Galaxy. Observations of [N II]/Hα and [S II]/Hα line ratios in the interarm region have a smaller increase with decreasing Hα intensity. However, due to the low Hα intensity at large $|z|$ in our simulations where the density is very small, we are still unable to match these ratios. There is a significant difference between the line ratios from regions below and above the mid-plane in the simulations and is attributed to the asymmetric density structure in the MHD simulation (see Fig. 1). It is notable that we have assumed a path length through our simulations of 1 kpc; however, this is an arbitrary choice. If we adopt a path length of 2 kpc, then the Hα intensity would be twice as large, and therefore closer to that observed in the Perseus Arm, while leaving the line ratios unchanged.

We have been unable to produce any increase in [S II]/Hα towards low Hα intensities even with an additional heating term. The difficulty in reproducing observations of S lines is not unexpected and is most likely because the dielectronic recombination rates for S are unknown. Most photoionization codes either ignore dielectronic recombination for S or, as employed here, use averages of the rates for C, N, and O neglecting any temperature dependence (Ali et al. 1991).

4.2 Temperature

With the assumption that N is primarily in the singly-ionized state throughout the DIG, observations of the line ratios in the Perseus Arm have been analysed to determine the temperature structure in the gas indicating that it rises from around 7000 K at $|z| = 0.75$ kpc to over 10 000 K above $|z| = 1.75$ kpc (Haffner et al. 1999; Madsen et al. 2006). In Fig. 6, we present the average temperature of ionized material in our simulations with and without the additional heating term, G_1. To produce Fig. 6, we have applied a cut where cells with temperature over 30 000 K in the MHD simulations (typically corresponding to density below $\approx 5 \times 10^{-4}$ cm^{-3}) have been neglected. These cells represent parts of 'bubbles' in the MHD simulations which in reality will be shock-heated and collisionally ionized, processes that we do not consider in our current pure photoionization models.

Fig. 6 shows that without the addition of a non-photoionization heating term, we are unable to reproduce the inferred increase
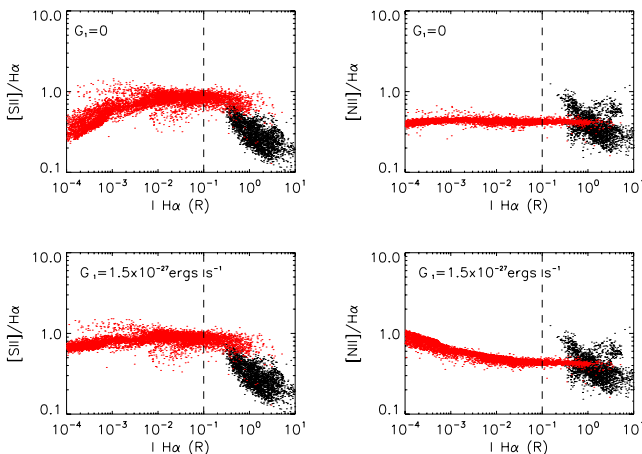

Figure 5. Emission line ratios showing [N II]/Hα and [S II]/Hα versus Hα intensity for MHD simulations with $Q_{49} = 1$ (red points) compared with WHAM data from the inter arm region (black points). The vertical line represents the WHAM sensitivity limit. Upper and lower panels show simulations without and with additional heating, respectively.
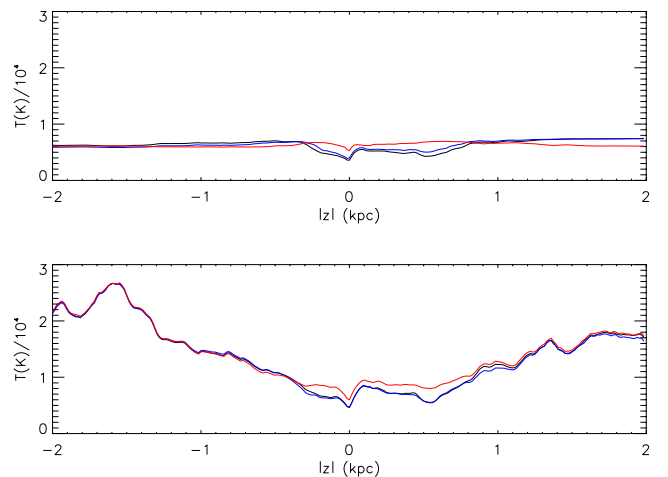

Figure 6. Average vertical temperature structure of photoionized gas in simulations with (top panel) no additional heating and (bottom panel) additional heating $G_1 n_e = 1.5 \times 10^{-27}$ erg s^{-1} n_e for ionizing luminosities. $Q_{49} = 10$ (red), 1(blue), 0.5 (black).

in temperature with height. However, once additional heating ($G_1 n_e = 1.5 \times 10^{-27} n_e$ erg cm^{-3} s^{-1}) has been added, we do reproduce this increase. We find that this increase is larger than inferred by Haffner et al. (1999), with the gas temperature increasing to above 17 000 K at 1.75 kpc because of the very small densities for $|z| \gtrsim 300$ pc in the MHD simulation. A smaller value for G_1 gives lower temperatures but does not give a noticeable increase of [N II]/Hα at low n_e. There is a significant difference between the line ratios from regions below and above the mid-plane in the simulations and is attributed to the asymmetric density structure in the MHD simulation (see Fig. 1).

5 FRACTAL MODEL OF THE ISM

In the previous section, we have shown that photoionization models of a turbulent ISM can reproduce general trends in Hα emission observed in the Galactic DIG, and that to increase emission line ratios an additional heating component is required. However, due to the small scaleheight in the MHD simulations, the scaleheight of Hα is smaller than observed in the Perseus Arm of the Galaxy. As a guide for future MHD simulations of the Galactic ISM, in this section we explore the photoionization of analytic density structures that can better reproduce the observed average vertical distribution of Hα intensity and emission line ratios observed by WHAM.

We adopt a smooth, four-component ISM density structure comprising a Dickey–Lockman distribution plus a more vertically extended component to produce the Hα emission from the DIG. To allow ionizing photons from mid-plane OB stars to propagate to large heights, we turn the smooth density into a 3D fractal structure using the fractal algorithm of Elmegreen (1997) as described by Wood et al. (2005). We adopt the same five-level hierarchical clumping algorithm, casting 16 seeds at the first level and 32 at each subsequent level. The density structure is arranged so that 33 per cent of the mass is smoothly distributed with the remaining fraction in the hierarchical clumps. For further details of the algorithm, see fig. 4 of Wood et al. (2005) and the accompanying description.

A density structure that produces the observed scaleheight of Hα with an input ionizing luminosity of $Q_{49} = 16$ is

$$n(z) = 0.4 e^{-(|z|/h_1)^2/2} + 0.11 e^{-(|z|/h_2)^2/2}$$
$$+ 0.06 e^{-|z|/h_3} + 0.04 e^{-|z|/h_4}, \qquad (2)$$

where the height z is measured in pc and the number densities are per cm^3. The first three components represent the Dickey–Lockman distribution shown in Fig. 1 with scaleheights $h_1 = 90$ pc, $h_2 = 225$ pc, $h_3 = 400$ pc. The fourth term represents the low-density extended diffuse ionized gas and we take the scaleheight to be $h_4 = 1000$ pc, as typically inferred from Hα observations in the Galaxy.

As before, we place 24 ionizing sources in the simulation and assign each source a $T = 35\,000$ K model atmosphere spectrum corresponding to an O5II star (Underhill et al. 1979).

Fig. 7 shows the edge-on view of the Hα intensity and the neutral hydrogen column density for the fractal density structure described above. The low-density pathways of the interclump medium allow ionizing photons to reach and ionize gas many kpc from the mid-plane and the Hα intensity and [N II]/Hα line ratios shown in Figs 8–10 are similar to observed in the Perseus Arm. This is not surprising as we have adopted a density structure that will produce the intensity distribution of Hα in line with the analytic results presented by Haffner et al. (1999) and Reynolds et al. (1999). While the fractal models, with additional heating terms, reproduce many of the features in diagnostic line ratio plots, the Hα intensity map does
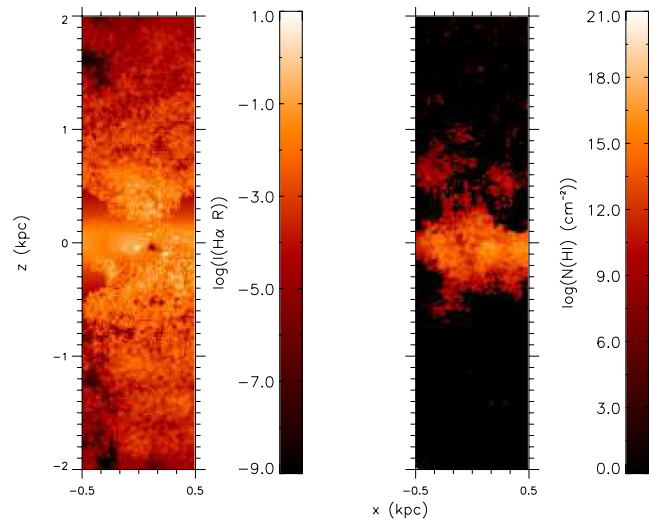

Figure 7. Edge-on view of Hα intensity (left) and column density of neutral hydrogen (right) for an analytic fractal model of the DIG.
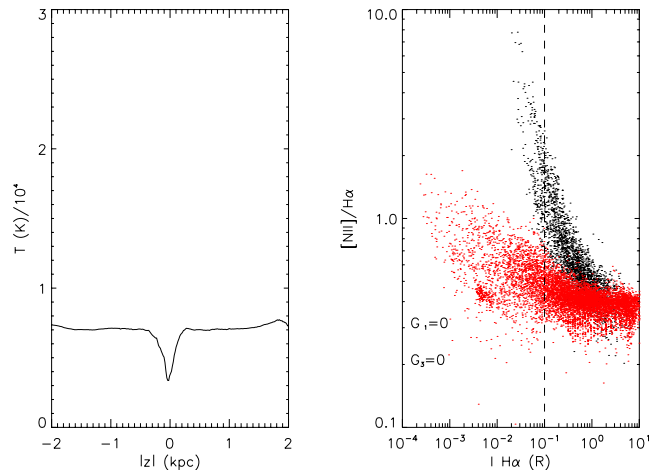

Figure 8. Analytic fractal model of the DIG. Left: average vertical temperature structure of ionized gas. Right: [N II]/Hα versus Hα for the Perseus Arm (black) and this model (red). The vertical line represents the WHAM sensitivity limit. Here, we show [N II]/Hα line ratios only in the region that corresponds to the Perseus Arm ($|z| < 1.8$ kpc). Although this model seems able to reproduce the observed Hα and neutral H, [N II]/Hα and temperature are different to those expected, suggesting the need for an additional heating term to increase temperature and [N II]/Hα at large $|z|$.

not exhibit the filamentary structures, loops, and bubbles present in the MHD simulations. Therefore, the fractal models should serve as a guide for the average density structure and additional heating required for future MHD simulations of the ISM and DIG.

The resulting average temperature structure and [N II]/Hα versus Hα are shown for simulations with no additional heating (Fig. 8), additional heating proportional to n_e (Fig. 9) with $G_1 = 4 \times 10^{-26}$, and an additional heating term to simulate cosmic ray heating (Fig. 10) parametrized by

$$G_3 = 1.2 \times 10^{-29} e^{-3|z|/4000\,\text{pc}} \text{ erg cm}^{-3} \text{ s}^{-1}, \qquad (3)$$

as in equation (1). This equation for cosmic ray heating was determined by Wiener et al. (2013) via analytic modelling of the [N II] and Hα emission and assuming that N$^+$/H$^+$ is constant in the DIG and assuming a 1D density structure. G_3 is 100 times smaller than
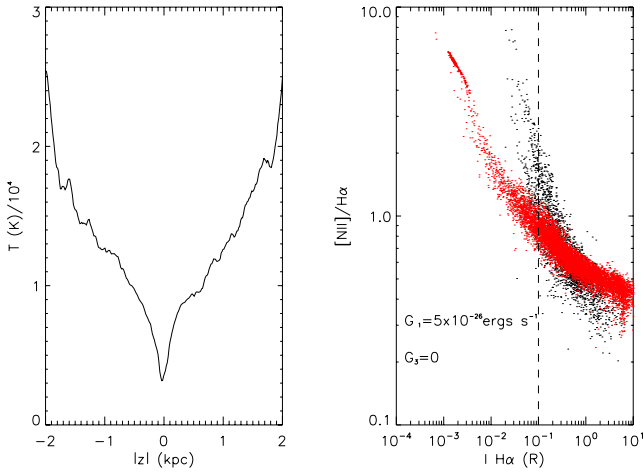
Figure 9. Same as Fig. 8 including additional heating $G_1 = 4 \times 10^{26}$. This model is now able to produce [N II]/Hα and temperatures similar to those inferred. Here, we show [N II]/Hα line ratios only in the region that corresponds to the Perseus Arm ($|z| < 1.8$ kpc).
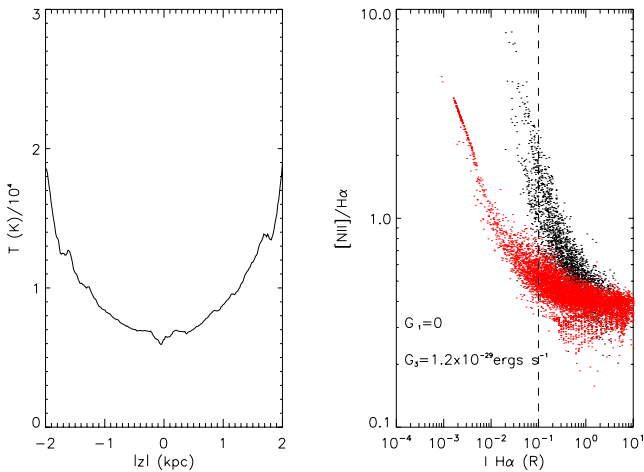

Figure 10. Same as Fig. 8 including additional heating from cosmic rays G_3 from equation (3). Here, we show [N II]/Hα line ratios only in the region that corresponds to the Perseus Arm ($|z| < 1.8$ kpc.)

the value found by Wiener et al. (2013), because our simulations determine the actual ionization fractions, and include the spatial variation of ionization, heating and cooling due to the 3D density, radiation field, and temperature structure. Modelling data using our 3D photoionization code therefore provides a better estimate of the additional heating terms required to reproduce the observed trends in the diagnostic diagrams.

6 HOW FAR CAN PHOTONS TRAVEL TO IONIZE THE DIG?

How far photons are able to travel through the ISM and ionize the DIG is a question that is important to studies not only of DIG in galaxies, but also for the escape of ionizing photons into the intergalactic medium. The 3D structures in the MHD and fractal density grids provide low-density pathways allowing ionizing photons to reach far above the mid-plane. Fig. 11 shows a histogram of the distances travelled by ionizing photons in the density structure provided by the MHD simulations. Some photons do indeed travel very large distances from their sources and are responsible for ionizing
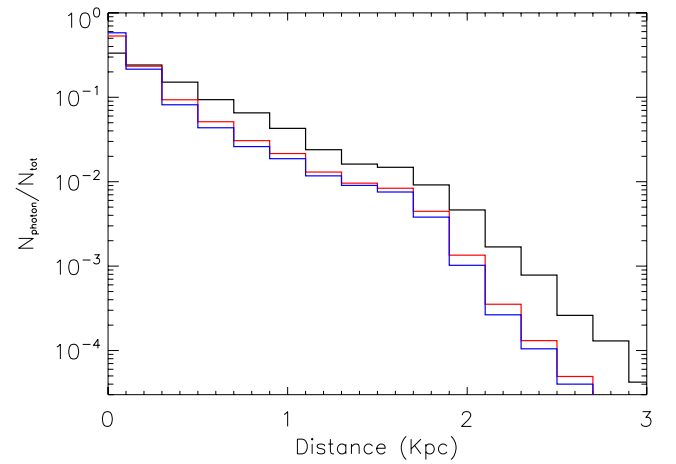

Figure 11. Histogram of distances travelled by ionizing photons through the MHD simulation grid for ionizing luminosities $Q_{49} = 10$ (black), 1 (red), 0.5 (blue).
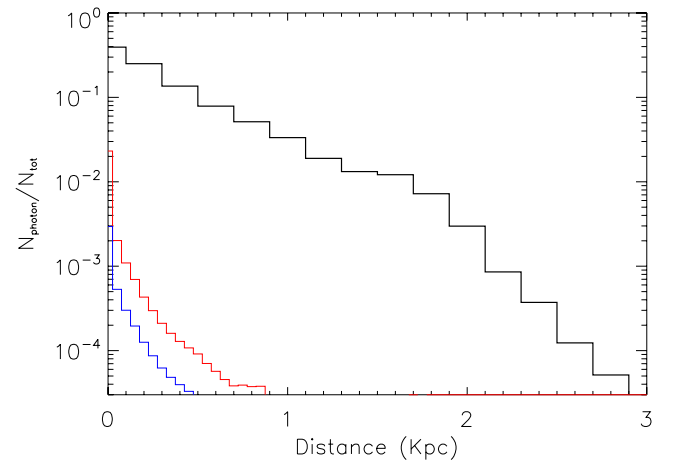

Figure 12. Histogram showing distances travelled by all ionizing photons (black), diffuse photons from hydrogen (red), and helium (blue) for $Q_{49} = 1$.

the gas at large $|z|$. The majority of the ionizing photons ionize denser gas towards the mid-plane and only a small fraction is required to ionize the low-density high-altitude gas. Increasing the ionizing luminosity allows photons to travel larger distances because more of the gas at low altitudes is ionized and hence presents a very small opacity.

Our photoionization code tracks direct stellar photons and also diffuse ionizing radiation from H and He recombination. The diffuse ionizing radiation consists of Lyman continuum from recombinations to the ground state of H and He, the He two-photon continuum, and the 19.8 eV line from He (Wood et al. 2004). Fig. 12 shows a histogram of the distances travelled by direct and diffuse ionizing photons and shows that the majority of the diffuse photons are absorbed close to their location of emission (i.e. the 'on the spot' approximation in many photoionization codes), but some do travel many hundreds of parsecs through the MHD density grid.

Fig. 13 shows the mean intensity of the ionizing photons in a one pixel wide slice of the simulation box compared to the density in that slice with positions of 'bubbles' marked with a star. Photons travel primarily in the low-density regions of the grid at high altitude, but close to the mid-plane they travel primarily in bubbles or structures attached to these bubbles. The brightest regions in the
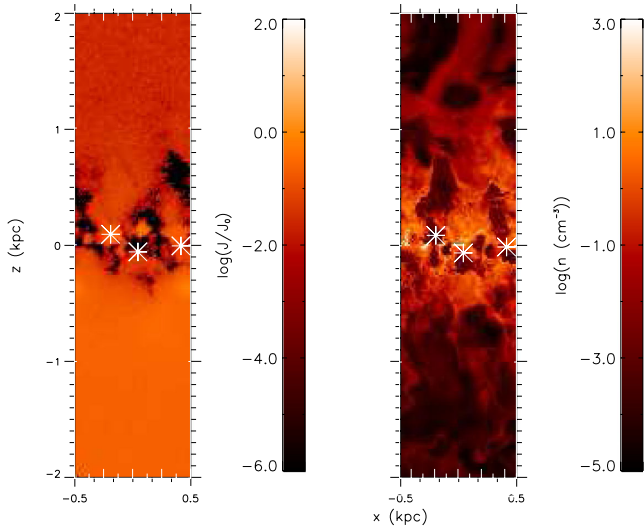
Figure 13. Maps showing mean intensity of ionizing radiation (left) and density (right) in one slice of the simulation box. White stars indicate the position of 'bubbles' in the MHD simulations and are characterized by low-density regions in the density structure (right). Bright regions of intensity show areas in which many photons are travelling while dark regions have few photons entering them. There is a strong relation between the density of the region and the number of photons travelling in that gas with low-density regions having many photons in them and high-density regions appearing dark in mean intensity.

mean intensity map correspond to source locations, and in the case where a source has been randomly placed in a high-density region close to the mid-plane, its ionizing photons are trapped close to the source. At higher altitudes the mean intensity becomes more uniform but higher density regions are still visible with fewer photons penetrating into and through these cells. All of the 'bubbles' in the simulations are located close to the mid-plane of the box and so at high altitudes photons appear to be travelling through a low-density medium. This provides further evidence that compared to a smooth density structure a 3D ISM naturally allows for ionizing photons to penetrate to larger distances and produce widespread diffuse ionized gas.

7 CONCLUSIONS

We have produced photoionization simulations of the DIG in an environment similar to that in the outer disc of a spiral galaxy and compared these to observations of the Perseus Arm and an interarm region in the solar neighbourhood. We summarize our main conclusions here.

(i) The photoionization of 3D density structures from MHD simulations naturally produces widespread diffuse ionized gas with a density scaleheight larger than that of neutral hydrogen. However, the density grids from the MHD simulations we have used here have a low scaleheight resulting in smaller $H\alpha$ intensity scaleheight than observed in the Perseus Arm.

(ii) We find that with the addition of a heating term, such as heating by cosmic rays or dissipation of turbulence, our simulations are able to reproduce general trends in [N II]/$H\alpha$ optical emission line ratios in the DIG.

(iii) A fractal density structure for the ISM with higher density at large |z| than in the MHD simulations better reproduces WHAM

observations of the Perseus Arm. This will provide a guide for the required density structure for future MHD simulations of the DIG.

(iv) Finally, our simulations demonstrate that ionizing photons are able to travel many kiloparsecs to ionize the DIG at large heights above the mid-plane, with photons travelling through low-density 'bubbles' close to the mid-plane and through low-density diffuse gas at large heights.

An important next step in modelling the ionization of the DIG will be to include photoionization as a dynamical process in MHD simulations of the gas (e.g. de Avillez et al. 2012). This may increase the density of gas at large heights since photoionization will increase the temperature of the gas and allow the gas to expand to a larger height, thereby sustaining higher densities above the mid-plane of the Galaxy that are demanded by the WHAM observations.

ACKNOWLEDGEMENTS

REFERENCES

Ali B., Blum R. D., Bumgardner T. E., Cranmer S. R., Ferland G. J., Haefner R. I., Tiede G. P., 1991, PASP, 103, 1182

Armstrong J. W., Rickett B. J., Spangler S. R., 1995, ApJ, 443, 209

Barger K. A., Haffner L. M., Bland-Hawthorn J., 2013, ApJ, 771, 132

Bland-Hawthorn J., Freeman K. C., Quinn P. J., 1997, ApJ, 490, 143

Burkhart B., Lazarian A., Gaensler B. M., 2012, ApJ, 749, 145

Chepurnov A., Lazarian A., 2010, ApJ, 710, 853

Cox D. P., 2005, ARA&A, 43, 337

Daflon S., Cunha K., de la Reza R., Holtzman J., Chiappini C., 2009, AJ, 138, 1577

de Avillez M. A., 2000, MNRAS, 315, 479

de Avillez M. A., Asgekar A., Breitschwerdt D., Spitoni E., 2012, MNRAS, 423, L107

Dickey J. M., Lockman F. J., 1990, ARA&A, 28, 215

Elmegreen B. G., 1997, ApJ, 477, 196

Fryxell B. et al., 2000, ApJS, 131, 273

Gaensler B. M., Madsen G. J., Chatterjee S., Mao S. A., 2008, PASA, 25, 184

Garmany C. D., Conti P. S., Chiosi C., 1982, ApJ, 263, 777

Haffner L. M., Reynolds R. J., Tufte S. L., 1999, ApJ, 523, 223

Haffner L. M., Reynolds R. J., Tufte S. L., Madsen G. J., Jaehnig K. P., Percival J. W., 2003, ApJS, 149, 405

Haffner L. M. et al., 2009, Rev. Mod. Phys., 81, 969

Harfst S., Theis C., Hensler G., 2006, A&A, 449, 509

Hausen N. R., Reynolds R. J., Haffner L. M., Tufte S. L., 2002, ApJ, 565, 1060

Hill A. S., Benjamin R. A., Kowal G., Reynolds R. J., Haffner L. M., Lazarian A., 2008, ApJ, 686, 363

Hill A. S., Joung M. R., Mac Low M.-M., Benjamin R. A., Haffner L. M., Klingenberg C., Waagan K., 2012a, ApJ, 750, 104

Hill A. S., Joung M. R., Mac Low M.-M., Benjamin R. A., Haffner L. M., Klingenberg C., Waagan K., 2012b, ApJ, 761, 189

Hoyle F., Ellis G. R. A., 1963, Aust. J. Phys., 16, 1

Jenkins E. B., 2009, ApJ, 700, 1299

Joung M. K. R., Mac Low M.-M., 2006, ApJ, 653, 1266

Joung M. R., Mac Low M.-M., Bryan G. L., 2009, ApJ, 704, 137

Kim J.-h., Krumholz M. R., Wise J. H., Turk M. J., Goldbaum N. J., Abel T., 2013, ApJ, 775, 109

Kuijken K., Gilmore G., 1989, MNRAS, 239, 605

Kulsrud R. M., Zweibel E. G., 2008, Rep. Prog. Phys., 71, 046901

McKee C. F., Ostriker J. P., 1977, ApJ, 218, 148

Mac Low M.-M., Klessen R. S., 2004, Rev. Mod. Phys., 76, 125

Madsen G. J., Reynolds R. J., 2005, ApJ, 630, 925

Madsen G. J., Reynolds R. J., Haffner L. M., 2006, ApJ, 652, 401

Maíz-Apellániz J., 2001, AJ, 121, 2737

Mathis J. S., 2000, ApJ, 544, 347

Miller W. W., III, Cox D. P., 1993, ApJ, 417, 579

Minter A. H., Spangler S. R., 1997, ApJ, 485, 182

Navarro J. F., Frenk C. S., White S. D. M., 1996, ApJ, 462, 563

Osterbrock D. E., Ferland G. J., 2006, Astrophysics of Gaseous Nebulae and Active Galactic Nuclei. University Science Books, Mill Valley, CA

Otte B., Gallagher J. S., III, Reynolds R. J., 2002, ApJ, 572, 823

Pauldrach A. W. A., Hoffmann T. L., Lennon M., 2001, A&A, 375, 161

Peters T., Klaassen P. D., Mac Low M.-M., Klessen R. S., Banerjee R., 2012, ApJ, 760, 91

Rand R. J., 1998, ApJ, 501, 137

Reynolds R. J., 1990, ApJ, 349, L17

Reynolds R. J., Hausen N. R., Tufte S. L., Haffner L. M., 1998, ApJ, 494, L99

Reynolds R. J., Haffner L. M., Tufte S. L., 1999, ApJ, 525, L21

Savage B. D., Wakker B. P., 2009, ApJ, 702, 1472

Simpson J. P., Rubin R. H., Colgan S. W. J., Erickson E. F., Haas M. R., 2004, ApJ, 611, 338

Sternberg A., Hoffmann T. L., Pauldrach A. W. A., 2003, ApJ, 599, 1333

Underhill A. B., Divan L., Prevot-Burnichon M. L., Doazan V., 1979, in Conti P. S., De Loore C. W. H., eds, Proc. IAU Symp., Vol. 83, Mass Loss and Evolution of O-Type Stars. Reidel, Dordrecht, p. 103

Vacca W. D., Garmany C. D., Shull J. M., 1996, ApJ, 460, 914

Wiener J., Zweibel E. G., Oh S. P., 2013, ApJ, 767, 87

Williams J. P., McKee C. F., 1997, ApJ, 476, 166

Wolfire M. G., Hollenbach D., McKee C. F., Tielens A. G. G. M., Bakes E. L. O., 1995, ApJ, 443, 152

Wood K., Mathis J. S., 2004, MNRAS, 353, 1126

Wood K., Mathis J. S., Ercolano B., 2004, MNRAS, 348, 1337

Wood K., Haffner L. M., Reynolds R. J., Mathis J. S., Madsen G., 2005, ApJ, 633, 295

Wood K., Hill A. S., Joung M. R., Mac Low M.-M., Benjamin R. A., Haffner L. M., Reynolds R. J., Madsen G. J., 2010, ApJ, 721, 1397

Zurita A., Rozas M., Beckman J. E., 2000, A&A, 363, 9

Zurita A., Beckman J. E., Rozas M., Ryder S., 2002, A&A, 386, 801

This paper has been typeset from a TeX/LaTeX file prepared by the author.